Composite Interfaces, Vol. 15, No. 4, pp. 363–377 (2008)

Also available online - www.brill.nl/ci

Influence of material processing and interface on the fiber fragmentation process in titanium matrix composites

THEODORE E. MATIKAS *

Department of Materials Science and Engineering, University of Ioannina, University Campus, 45110 Ioannina, Greece

Received 4 June 2007; accepted 19 June 2007

Abstract—The objective of this work is to study the effect of composite processing conditions on the nature of the fiber–matrix interface in titanium matrix composites and the resulting fragmentation behavior of the fiber. Titanium matrix, single fiber composites (SFCs) were fabricated by diffusion bonding and tensile tested along the fiber axis to determine their interfacial load transfer characteristics and the resulting fiber fragmentation behavior. Two different titanium alloys, Ti-6Al-4V (wt%) and Ti-14Al-21Nb (wt%), were used as matrix material with SiC (SCS-6) fibers as reinforcement. The tensile tests were conducted at ambient temperature and were continuously monitored by acoustic emission. It was observed that the Ti-6Al-4V/SCS-6 composite system exhibited a greater degree of fiber–matrix interfacial reaction, as well as a rougher interface, compared to Ti-14Al-21Nb/SCS-6 composites. Acoustic emissions during tensile testing showed that most of the fiber fractures in Ti-6Al-4V/SCS-6 occurred at strains below ∼5% and the fragmentation ceased at ∼10% strain corresponding to specimen necking. In contrast, the Ti-14Al-21Nb/SCS-6 composite deformed without necking and fiber fractures occurred throughout the plastic range until final fracture of the specimen at about 12% strain. The markedly different fragmentation characteristics of these two composites were attributed to differences in the fiber–matrix interfacial regions and matrix deformation behavior.

Keywords: Titanium alloys; metal matrix composites; fiber–matrix interface; fragmentation.

1. INTRODUCTION

Several test methods are currently available for quantifying the interfacial properties of metal matrix composites (MMCs). In particular, techniques for measuring the interfacial shear properties of continuously reinforced MMCs include the thin slice fiber push-out (indentation), fiber pull-out, transverse, and fiber fragmentation tests. This paper deals with the characterization of fiber–matrix interfacial behavior in fiber-reinforced titanium alloy composites using the fiber fragmentation technique.

*E-mail: matikas@otenet.gr

Early work of Kelly and Tyson [1] on W fiber-reinforced Cu matrix composites suggested that reinforcement effect would occur when the volume fraction of fibers is above a critical value and multiple fracture or fragmentation of fibers would take place when the fiber volume fraction is below a certain minimum value. On this basis, the study of fiber fragmentation requires testing of composite specimens with a relatively low volume fraction of fibers. The test which is most commonly performed is the single fiber fragmentation (SFF) test in which a dog bone-shaped specimen consisting of an isolated fiber embedded in a matrix material is loaded in tension along the fiber axis. Load transfer from matrix to fiber by interfacial shear parallel to the fiber axis produces a tensile stress in the fiber that is nominally uniform within the section away from the fiber ends. As the applied strain increases, the fiber breaks repeatedly into smaller fragments and the fiber stress decays to zero near these breaks. With continued loading, fragments longer than a certain critical length will experience an increasing, uniform stress only over their center sections, which are susceptible to further breakage. In practice, however, the SFF test usually results in a wide distribution of fragment lengths since the strength of fiber fragments depends on their length [2, 3]. Therefore, the determination of interfacial shear strength using fragment length data is more complicated as discussed elsewhere [2–5]. In spite of these complexities, the SFF test has been widely applied since it allows simulation of the interfacial load transfer occurring in real composite specimens subjected to longitudinal tensile loading and closely approximates the chemical and thermo-mechanical effects present at the interfaces of real composites.

Although the single fiber fragmentation test was first performed on MMCs during the early 1960s [1], the subsequent application of this test was primarily limited to transparent polymer composites due to the ease of their preparation and observation of the fiber fragments using birefringence techniques [2–11]. There has also been an interest in the application of this test to model MMCs, such as W fiber-reinforced Cu as well as SiC fiber-reinforced Al and Ti alloy matrix composites, using various techniques, including acoustic emission monitoring [12–17].

Ochiai and Osamura [12] tested a number of single W fiber-reinforced Cu matrix composite specimens with different thickness and showed that the average fragment length increased with increasing volume fraction of the fiber. While there is no provision in the Kelly equation to account for this result, Ochiai and Osamura assumed that the fiber strength is described by Weibull distribution and performed a computer simulation, which gave a fairly good prediction of the observed dependence of fragmentation on fiber volume fraction [12]. Molliex *et al.* [13] studied fragmentation in SiC (SCS-2) fiber-reinforced aluminum alloy composites and concluded that interfacial stress transfer in these MMCs is limited by the plastic deformation of the matrix alloy. Clough *et al.* [14] and Houpert *et al.* [15] conducted SFF tests on SiC fiber-reinforced single crystal Al and Al_2O_3 fiber-reinforced Cu matrix composites, respectively, and analyzed the results in terms of the load drops corresponding to fiber fragmentation.

Studies dealing with fiber fragmentation in titanium-based composites are limited. Vassel *et al*. [13, 16] and Le Petitcorps *et al*. [17] conducted SFF tests on Ti-6Al-4V matrix composites containing different types of silicon carbide fibers. Although the matrix deformation behavior and evolution of fragmentation observed in these two studies were somewhat different, they reported very similar fragment lengths and interfacial shear strength values in the corresponding composite systems. The reasons for the reported similarities are not clear. These past studies were concerned primarily with the estimation of the interfacial shear strength values using the observed fragment length data. Clearly, there is a need to understand the influence of interface microstructure and constituent properties on shear load transfer and fiber fragmentation. The present study of fiber fragmentation in titanium-based composites deals with the determination of the effects of fiber–matrix interfacial reaction and matrix deformation characteristics on fiber fragmentation behavior.

2. EXPERIMENTAL PROCEDURE

2.1. Processing of single fiber composites

The starting materials used in this work were Ti-6Al-4V and Ti-14Al-21Nb alloy sheets, and Textron's SCS-6 SiC fibers. It should be noted that the Ti-14Al-21Nb (wt%) alloy is commonly referred to as Ti-24Al-11Nb, based on its composition in at%. The single fiber composite samples were fabricated by diffusion bonding of a fiber placed between matrix alloy sheets at temperatures below the β transus of the alloys using two different processing routes: (1) A two-step process involving vacuum hot pressing at 925°C under 5.5 MPa pressure for 30 min followed by hot isostatic pressing (HIP'ing) at 985°C under 100 MPa pressure for 2 h, and (2) A single-step consolidation process involving vacuum hot pressing at 954°C under a pressure of 9.2 MPa for 30 min. The composite panels fabricated by these two routes are designated as Type A (two-step process) and Type B (single-step process) samples, respectively.

The preforms for vacuum hot pressing consisted of a SCS-6 fiber sandwiched between the titanium alloy sheets. The Ti-6Al-4V alloy sheets used were 80 mm $\times$ 30 mm $\times$ 1.25 mm thick, whereas the Ti-14Al-2lNb sheets were 75 mm $\times$ 25 mm $\times$ 0.5 mm thick. Because of the finer gage of the Ti-14Al-2lNb material, two sheets of this alloy were used on each side of the fiber. A fiber segment equal to the length of the alloy sheets was centered and aligned parallel to the length of the preform by applying a very small amount of a fugitive organic binder to its two ends. Two different techniques were used to minimize any mechanical damage to the fiber coating during handling of the preform and the initial loading operation, depending on the processing route. The preforms used for consolidating the Type A samples included two 75 mm long $\times$ 6 mm wide strips of a SiC fiber mat, each containing about 20 evenly spaced fibers, which were placed symmetrically on the two sides of the central fiber and at a distance of about 5 mm from the centerline. In the case

of the Type B samples, the fiber was placed in a 0.15 mm deep groove, which was machined in one of the alloy sheets. The preforms were placed inside a rectangular steel can with inner dimensions of 82 mm × 32 mm, and a 3.2 mm wall thickness. All samples were soaked for 15 min at the consolidation temperature before the load was applied during vacuum hot pressing. In the case of the Type A samples, the vacuum hot-pressed material was encapsulated in evacuated steel cans prior to HIP'ing. While most of the composite samples contained a long fiber segment, a few samples were also prepared using several short fiber segments, each measuring ∼5 mm in length, for comparison.

Metallographic sections were taken normal to the fiber axis to examine the fiber–matrix interface region. The consolidated composite panels were machined into 1.5 mm thick dog-bone type tensile specimens with 19.0 mm × 6.4 mm gage sections having a fiber volume fraction of ∼0.16%. All test specimens were examined by microfocus X-ray radiography to ascertain proper alignment of the fiber parallel to the tensile specimen axis.

2.2. Mechanical testing and acoustic emission monitoring

Tensile tests were conducted on a servohydraulic machine in laboratory air at ambient temperature using a nominal strain rate of 2×10^{-4} s^{-1} for both Ti-6Al-4V/SCS-6 and Ti-14Al-21Nb/SCS-6 composite specimens. The results reported here are based on test data from at least two specimens in each microstructural condition. Tensile loading was continued until fracture of the specimen in most of the tests. A few tests were interrupted at intermediate strains to determine the evolution of fragmentation as a function of specimen strain.

Acoustic emission (AE) activity was monitored during tensile testing by employing a broadband resonant transducer with a nominal center frequency of 250 kHz, which was coupled via high vacuum grease to the flat gage section of the samples. Transducer outputs were amplified first by 40 dB using a preamplifier with a bandpass filter of 100–400 kHz and then by an additional 20 dB at the main amplifier. Some of the AE waveform parameters (peak amplitude, duration, etc.), as well as appropriate stress, strain and RMS voltage of the amplified transducer outputs, measured using an RMS voltmeter, were recorded by a computerized data acquisition system. The amplitude threshold was set at 55 dB based on the acoustic response of monolithic titanium alloy specimens in a similar manner [18].

2.3. Metallographic examination of fiber–matrix interface and fiber fragmentation

The tested specimens were sectioned and polished parallel to the fiber axis using standard metallographic specimen preparation techniques. The delineation of fiber fragments was based primarily on sectioning of the single fiber composite specimens parallel to the fiber axis. Even small deviations from parallelism between the polishing surface and the fiber axis led to problems in retaining all fragments on the polished surface. Therefore, the grinding and polishing steps were carefully

controlled to prevent any loss of fragments during the metallographic specimen preparation. Additionally, some of the samples were electropolished to expose all the fragments using a solution of 500 ml methanol, 300 ml butyl cellosolve and 30 ml perchloric acid at $-40°C$ under 15 mA current and a potential of 18 V. Metallographic examination of fiber fragments and interfacial regions was conducted by using optical microscopy and SEM. Fractographic evaluation of the tested specimens was also conducted using SEM.

The extent of fiber–matrix reaction in the composite samples was characterized by metallographic examination of their cross-sections. Further, fibers were extracted from some composite specimens by chemically dissolving the matrix alloy in a solution of 5% HNO_3, 10% HF and 85% H_2O (by volume), and their surfaces were examined using SEM.

3. RESULTS AND DISCUSSION

Figure 1 presents a microfocus X-ray radiograph of the gage section of a Ti-6Al-4V/SCS-6 composite specimen showing fiber alignment with the tensile axis. The alignment of fiber was significantly improved when the SFC specimens were consolidated by using fiber retention grooves in the titanium alloy sheets.

3.1. Microstructure of the interface region

3.1.1. Type A composites (two-step process). The fiber–matrix interfacial regions of Ti-6Al-4V/SCS-6 and Ti-14Al-21Nb/SCS-6, Type A, single fiber composites, which were consolidated by the two-step process, are shown in Fig. 2.

The Ti-6Al-4V matrix presented an $(\alpha + \beta)$ two-phase structure with equiaxed α grains (5–10 μm grain size) and elongated β phase at α grain boundaries as well as grain interiors. The Ti-14Al-21Nb matrix consisted of a $(\alpha_2+\beta)$ two-phase structure with somewhat finer equiaxed α_2 grains (about 5 μm grain size) with less elongated β-phase at α_2 grain boundaries. It is evident that the fiber–matrix interfacial regions in these two composites are distinctly different. It is particularly important to note the changes that have occurred in the fiber coating. It should be noted that the microstructure of the SCS-6 SiC fiber has been previously characterized in detail

Figure 1. Microfocus X-ray radiograph showing the gage section of a Ti-6Al-4V/SCS-6 single fiber composite tensile specimen.

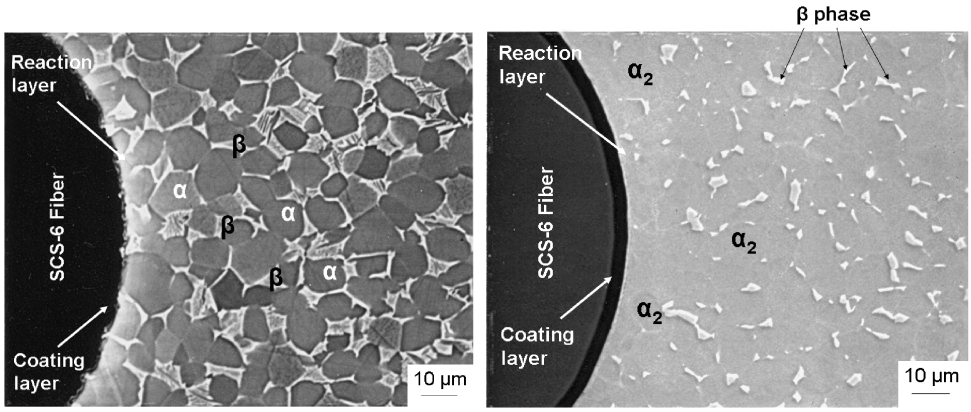

(a) (b)

Figure 2. SEM micrographs showing the fiber–matrix interfacial region, where the reaction and coating layers are visible, of Type A single fiber composite systems consolidated by a two-step process: (a) Ti-6Al-4V/SCS-6 with equiaxed α grains and elongated β phase at α grain boundaries, (b) Ti-14Al-21Nb/SCS-6 with equiaxed α_2 grains and less elongated β phase.

using TEM and other techniques [19]. This fiber has a coating measuring ∼3 μm in thickness and consisting of two main layers made up of turbostratic carbon matrix containing SiC particles. It has been shown that the inner and outer layers are 1.7 μm and 1.3 μm thick, respectively, and are separated by a very thin (∼100 nm) transition layer of carbon [19].

The Ti-6Al-4V/SCS-6 system exhibited a significant reaction zone with a very rough interface, which was produced due to preferential reaction between the β-phase of the matrix alloy and the carbon-rich coating layers of the fiber. As Fig. 2 shows, this reaction zone is composed of two layers with non-uniform thickness. Based on previous work [20, 21], these two layers are characterized as TiC and Ti_5Si_3, respectively. Much of the outer, carbon-rich layer of the SCS-6 fiber coating was consumed by this reaction, and a part of its inner, carbon-rich layer, was also attacked by the matrix at several locations along the fiber. In contrast, the Ti-14Al-21Nb/SCS-6 composite showed a narrower (0.3–0.4 μm thick) and smoother interfacial reaction zone. However, this composite also showed that a wide region of the matrix adjacent to the fiber was devoid of the β phase. The formation of the reduced reaction zone consisting of complex carbides and silicides along with the presence of a wide β-depleted region in this composite is well documented in the literature [22]. Figure 2 also shows some voids near the fiber along the bond line of the Ti-14Al-2lNb matrix alloy sheets due to incomplete consolidation. The role of these defects to fiber fragmentation behavior will be discussed later.

3.1.2. Type B composites (single-step process). While the two-step processing resulted in complete consolidation of the Type A single fiber composites, the single-step processing of Type B samples involving vacuum hot pressing for a shorter

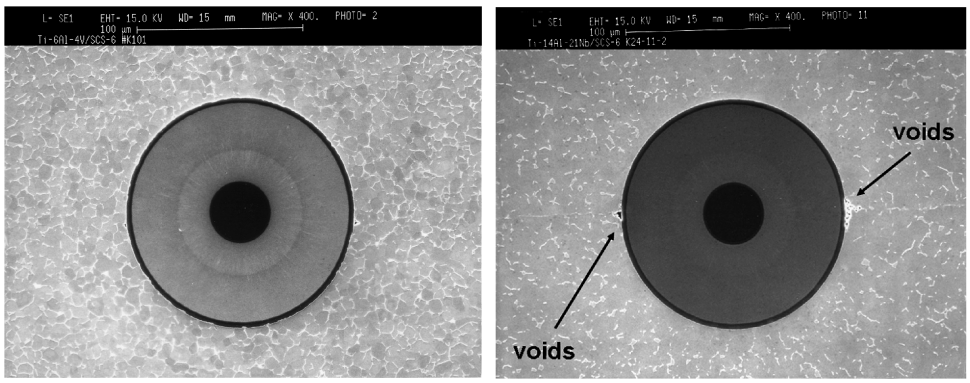

(a) (b)

Figure 3. SEM micrographs showing the fiber–matrix interfacial region of two Type B Ti-6Al-4V/SCS-6 single fiber composites, consolidated by the one-step process: (a) fully consolidated specimen, (b) specimen with remnant defects.

time at a lower temperature produced mixed results. The consolidation of Type B Ti-6Al-4V/SCS-6 composite was nearly complete and only small voids remained near the junction of the fiber and the bonding surfaces of the sheets. Figure 3a and 3b show the fiber–matrix interface regions of two such samples and illustrate the reproducibility of the microstructure. The size of the remnant voids was observed to differ slightly from sample to sample, as seen in these micrographs. In comparison to the Type A samples, the Type B Ti-6Al-4V/SCS-6 composite showed a significantly smoother fiber–matrix interface and a reduced reaction zone measuring $\sim$0.4 μm in thickness. This reaction involved only the outer carbon-rich coating of the fiber leaving the inner carbon-rich coating unaffected. On the other hand, the single step processing was inadequate for achieving full consolidation of the Ti-14Al-21Nb/SCS-6 composite, which showed delamination due to incomplete bonding of the matrix alloy sheets. Thus, the test results presented here concerning the processing effects deal primarily with the Ti6Al-4V/SCS-6 composite.

3.2. Fiber fragmentation testing at 23°C

3.2.1. Type A composites. Typical room temperature tensile stress–strain curves for the Ti-6Al-4V/SCS-6 and Ti-14Al-2lNb/SCS-6, Type A single fiber composites, which were consolidated by the two-step process, are shown in Fig. 4. The variation of the RMS voltage of the acoustic emission with strain is also shown in the figure. The Ti-6Al-4V/SCS-6 specimens displayed continuous yielding with high values of yield strength and elongation. This stress–strain behavior is consistent with the published tensile data for this alloy in the equiaxed ($\alpha + \beta$) microstructural condition. The Ti-14Al-21Nb/SCS-6 specimens exhibited a distinct yield point, yield drop and Luder's band formation, and deformed at much lower flow stresses as compared to the Ti-6Al-4V/SCS-6 composites. The elongation of the Ti-14Al-21Nb/SCS-6 SFC was still quite high and was attributed to the (0001) basal texture

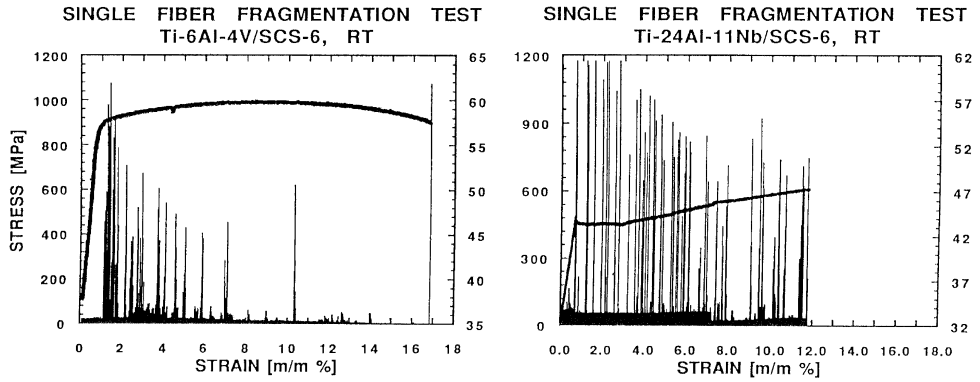

(a) (b)

Figure 4. Tensile stress–strain behavior and acoustic emission RMS voltage *vs* strain for the Type A single fiber composites tested at 23°C: (a) Ti-6Al-4V/SCS-6 and (b) Ti-14Al-21Nb/SCS-6.

of the α_2 phase in the matrix alloy sheet material used for fabricating the specimens. Similar results have been previously reported for a Ti_3Al-Nb alloy composed α_2 phase with a strong basal texture, which exhibited a high tensile elongation ($\sim$12%) at room temperature [22]. The enhanced ductility was explained in terms of the lower average orientation factor and lower grain boundary angles enabling the slip of <a> type dislocations, which are related to reductions in width of the specimen [23].

Typical AE RMS voltage *vs* elongation curves for these two composites are depicted in Fig. 4. No AE activity was observed during elastic straining of the two-step processed Ti-6Al-4V/SCS-6. However, marked AE activity was noted during elastic straining of the Ti-14Al-21Nb/SCS-6 composite. Similarly, high AE activity was observed at the onset of yielding in the case of Ti-14Al-21Nb/SCS-6 whereas little AE activity was detected at the yield of the Ti-6Al-4V/SCS-6 material. In both composites, a large number of sporadic high intensity AE bursts (events) commenced with the onset of plastic deformation. These AE events clustered immediately past the yield strain and then became less frequent. The peak amplitude of these bursts is high (>95 dB) and their duration ranges from 2 to 4 μs. These characteristics are significantly different from those of most of the signals detected during these tests indicating the operation of a distinct mechanism. No AE activity was observed after necking and prior to the fracture of the specimens. It is rather coincidental that the AE events occurred at about the same time as the onset of plasticity, since they are related to the energy released during a fiber fracture rather to the onset of plasticity.

Metallographic examination of the fibers in the two Type A composites, which were polished after tensile testing (Fig. 5) revealed that the single fiber had fragmented during straining. Fiber fracture behavior was found to be distinctly different in the two composite systems studied. The fiber fragments in Ti-14Al-21Nb/SCS-6 were significantly longer than those in Ti-6Al-4V/SCS-6. Both the

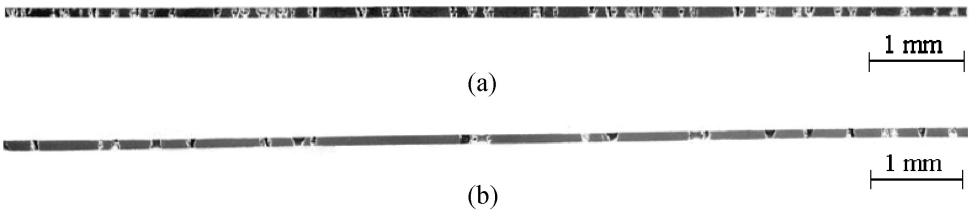

Figure 5. SEM micrographs showing fiber fragments in Type A single fiber composites tested at 23°C: (a) Ti-6Al-4V/SCS-6 and (b) Ti-14Al-21Nb/SCS-6.

composites revealed the presence of several short, secondary fiber ruptures between the longer primary fragments (Figs 6 and 7). The distinction between primary and secondary fiber ruptures using metallography was more difficult in the case of Ti-6Al4V/SCS-6 since the fragmentation occurred on a finer scale and resulted in severe shattering of the fiber with numerous secondary ruptures. However, metallographic evaluation of specimens from interrupted tensile tests confirmed the secondary fractures occurring between primary fragments. It is suggested that the secondary ruptures occur as a result of primary fiber fracture when stored elastic energy is released in the form of shock waves.

The primary and secondary fractures could also be distinguished on the basis of AE amplitude and event duration, with the primary fractures corresponding to high dB levels (>95 dB) and long durations (>2000 μs), and the secondary fiber cracking corresponding to low dB levels (<80 dB) and short durations (<2000 μs). In addition, some room temperature multiple cracking has been observed, as well as short duration (<2000 μs) AE events at the 90–95 dB range, which are fiber fractures occurring near the end of the test. Bare fiber tests also gave AE events >95 dB in amplitude and >2000 μs in duration corresponding to primary fiber fractures, as well as AE events <80 dB in amplitude and <2000 μs in duration, corresponding to secondary fiber cracking. The correlation between the AE events and the fragmentation events in the single fiber reinforced composites was examined by stopping a test after a given number of bursts and counting the number of fragments observed by metallography. The number of high amplitude AE events found to be identical to the number of fragments produced in the Ti-14Al-21Nb/SCS-6 composite sample. However, such a correlation could not be verified in the case of Ti-6Al-4V/SCS-6 since numerous secondary ruptures followed primary fragmentation events. The AE events do not always correspond to fiber fracture. When compared to Type A Ti-6Al-4V/SCS-6 SFC, the latter part of the stress–strain curves of Type A Ti-14Al-21Nb/SCS-6 SFC shows a lot of lower dB AE activity arising from matrix cracking, delamination along bond line (debonding), and reaction zone cracking, in addition to plastic deformation of the matrix.

On the basis of the AE characteristics of fiber fractures, it is observed that fragmentation attains saturation in the Ti-6Al-4V/SCS-6 Type A SFC specimens. The reason for achieving saturation in Ti-6Al-4V Type A SFC is the severity of fiber–matrix reaction and interface roughness causing extensive fracture. This is

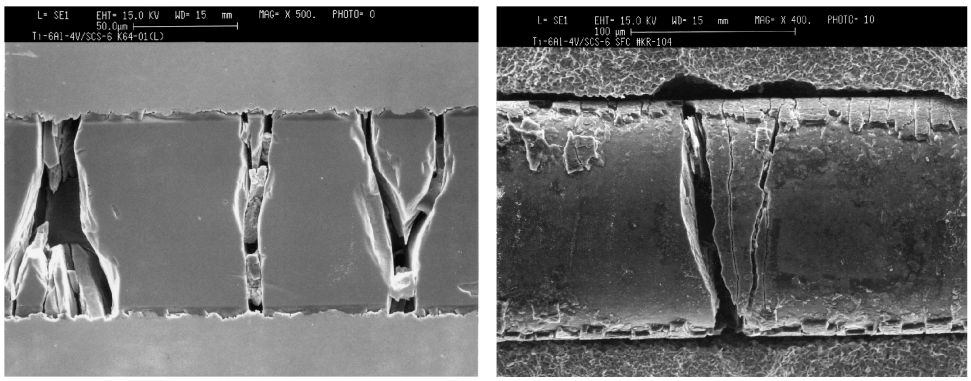

(a) (b)

Figure 6. SEM micrographs indicating fiber fracture, reaction zone cracking, and interface region in Ti-6Al-4V/SCS-6 single fiber composites following tensile testing at 23°C: (a) polished region and (b) electropolished surface.

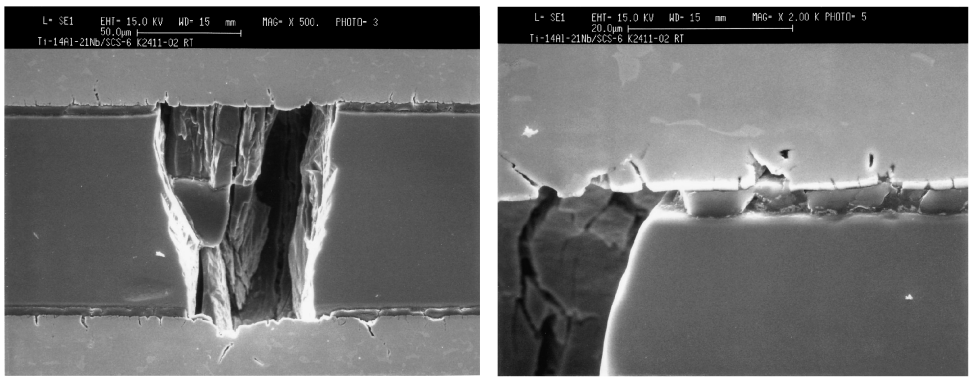

(a) (b)

Figure 7. SEM micrographs indicating fiber fracture, reaction zone cracking, and interface region in Ti-14Al-21Nb/SCS-6 single fiber composites following tensile testing at 23°C: (a) polished region and (b) electropolished surface.

not the case in the Type B Ti-6Al-4V. On the other hand, Ti-14Al-21Nb/SCS-6 composites do not attain saturation of fiber fragmentation. Typically, no saturation is observed in metal matrix composites and, from this point of view, the results from Ti-14Al-21Nb are not unusual. The occurrence of fragmentation is closely related to the work hardening rate (WHR) of the matrix material, since the fiber loading continues if WHR is high. Ti-14Al-21Nb/SCS-6 exhibits higher work hardening rate past yield than Ti-6Al-4V/SCS-6, which results in continued occurrence of high amplitude AE events in Ti-14Al-21Nb/SCS-6 samples. The yield stress and ultimate tensile strength of the Ti-14Al-21Nb matrix alloy are 521 MPa and 665 MPa, respectively, whereas yield stress and ultimate tensile strength of the Ti-6Al-4V matrix alloy is 890 MPa and 1010 MPa, respectively. This indicates

that fiber fracture continued until the end of the test, i.e. fragmentation does not saturate in this case. Other characteristics of Ti-14Al-21Nb/SCS-6 compared to Ti-6Al-4V/SCS-6, such as less fiber–matrix reaction, less degradation of SCS-6 fiber, formation of β-depleted layer, lower flow stress level, and shear localization, also play a role in absence of fragmentation saturation in this material. The different results obtained from various matrix materials, i.e. in Type A Ti-6Al-4V fragmentation ceases at around necking of the specimen, whereas in Ti-14Al-21Nb the WHR remains quite high throughout and, therefore, saturation is not attained, clearly demonstrate that the practice of stopping the test at some strain (i.e. 3% or 4%) as has been done in certain studies [17] is not justified.

In addition to the longer fragments and less secondary rupture, the Ti-14Al-21Nb/SCS-6 SFC specimens showed cracking of the β-depleted matrix layer near the interface, suggesting this cracking 'unloads' the fiber and results in fewer fiber fractures. Metallographic sections showed longer fragments with debonded interfaces at their ends and shorter fragments with a periodically cracked coating/reaction zone.

The significantly different fragmentation characteristics of the Ti-6Al-4V/SCS-6 and Ti14Al-21Nb/SCS-6, Type A, single fiber composites can be explained in terms of the fiber–matrix reaction and its effect on fiber strength in these two systems. Figure 8 shows SEM micrographs of the surface of extracted fibers from these two composites (Fig. 8a and 8c) along with fractographs of the fibers (Fig. 8b and 8d). In Ti-6Al-4V/SCS-6, extensive reaction at the fiber–matrix interface results in a rough interface due to the breaching of the fiber coating's outer layer and penetration into its inner layer. Consequently, there is a pronounced increase in the number of surface flaws on the fiber leading to severe degradation of the fiber strength. The strength of an SCS-6 fiber extracted from a Ti-6Al-4V/SCS-6 composite, measured for a 12 mm gage length, was found to be 3800 ± 350 MPa, whereas the strength of a virgin SCS-6 fiber was 4620 ± 300 MPa. Thus, tensile loading of this composite produces numerous fiber fractures and shattering of the fiber. This is consistent with the observation of surface crack initiation sites on the fiber fracture surface (Fig. 8b). In contrast, the fiber–matrix reaction in Ti-14Al-2lNb/SCS-6 is less severe and only part of the outer layer of the fiber coating is affected. The extracted fiber shows a smoother surface (Fig. 8c) and the fiber fracture surface shows internal initiation features, which are commonly observed (Fig. 8d). The strength of an SCS-6 fiber extracted from a Ti-14Al-2lNb/SCS-6 composite was found to be 4270 ± 350 MPa. Based on these data, it is reasonable to conclude that the surface flaw distribution of the fiber is not greatly affected in the Ti-14Al-21Nb/SCS-6 composite. Based on the severity of fiber–matrix reaction, one would expect higher strain for fiber in Ti-14Al-21Nb/SCS-6 as compared to Ti-6Al-4V/SCS-6. However, the reverse is true. The first fiber fracture occurs at a strain of 0.6–0.7% in Ti-14Al-21Nb/SCS-6 whereas this strain is much higher in Ti-6Al-4V/SCS-6 ($\sim$1% in Type A specimens and $\sim$1.4–1.5% in Type B specimens).

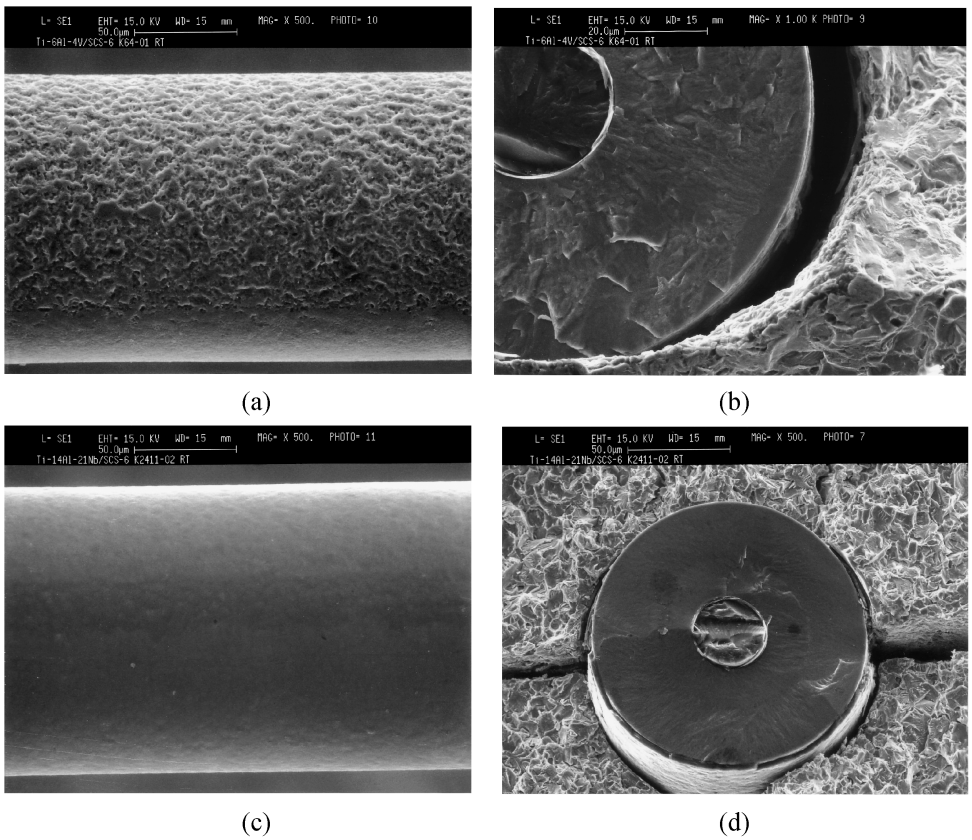

Figure 8. SEM micrographs showing the surface of fiber extracted from the composite and fractograph of Type A single fiber composites which were tensile tested at 23°C: (a), (b) Ti-6Al-4V/SCS-6 and (c), (d) Ti-14Al-21Nb/SCS-6.

3.2.2. Type B composites. As noted in Section 3.1.2, only the Ti-6Al-4V/SCS-6 SFC specimens were successfully consolidated by the single-step process. Thus, the test results presented in this paper, concerning Type B composites, deal primarily with the Ti6Al-4V/SCS-6 composite system.

Results from two different Ti-6Al-4V/SCS-6 SFC specimens, one fully consolidated, the other with remnant defects, indicated that processing can play an important role in the fragmentation behavior. Figure 9a shows very little AE activity during the elastic part of the stress–strain curve for a fully consolidated Ti-6Al-4V/SCS-6 SFC specimen, whereas Fig. 9b shows increased AE activity during the elastic part of the stress–strain curve for a Ti-6Al-4V/SCS-6 SFC specimen with remnant defects. A comparison of AE data from Ti-6Al-4V/SCS-6 SFC and Ti-14Al-21Nb/SCS-6 SFC tensile specimens also shows markedly different results during elastic loading (Figs 4 and 9). While Ti-14Al-21Nb/SCS-6 shows a large number of AE events during elastic loading with amplitudes in the range 55–85 dB, the Ti-6Al-4V/SCS-6 specimen shows only a couple of such events. It appears that

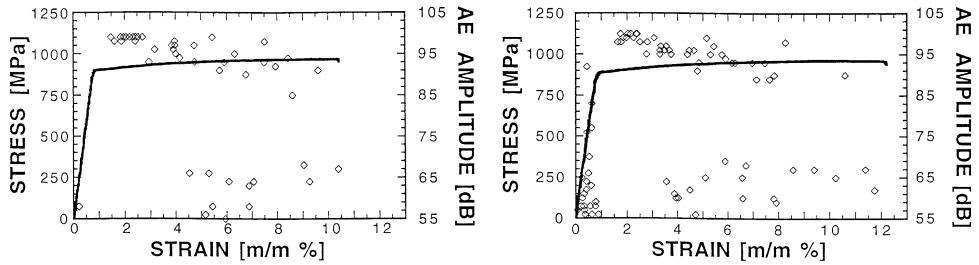

Figure 9. Tensile stress–strain behavior and acoustic emission amplitude *vs* strain for two Type B Ti-6Al-4V/SCS-6 single fiber composites tested at 23°C: (a) fully consolidated specimen; (b) sample with remnant defects.

this difference in AE activity during elastic loading arises from defects present in the specimen such as voids in the matrix due to poor consolidation (see Ti-14Al-21Nb/SCS-6 interface SEM — Fig. 3b). When voids are eliminated by proper consolidation, AE activity is absent in during elastic loading.

The fragmentation test of Type B Ti-6Al-4V/SCS-6 specimens shows longer fiber fragments than Type A Ti-6Al-4V/SCS-6 specimens. The number and length of the fragments was measured with metallography. Total number of all AE signals was found to be equal to the total number of fractures. Type B Ti-6Al-4V/SCS-6 SFC and Type A Ti-14Al-21Nb/SCS-6 SFC gave somewhat similar reaction zones and fragment lengths. It was found that the number of fragments increases with the increasing of the fiber–matrix reaction.

4. CONCLUSIONS

The present work showed markedly different fiber fragmentation behavior in Ti-6Al-4V/SCS-6 and Ti-14Al-21Nb/SCS-6 single fiber composite samples arising from differences in the fiber–matrix interface. The main results of this work are as follows.

Fragmentation characteristics are significantly affected by fiber–matrix reaction. Defects produced by this reaction at the fiber surface can lead to reduced fiber strength and result in extensive fragmentation of the fiber. This is influenced by matrix alloy composition as well as processing.

The frequency of occurrence of fiber fractures with increasing strain is shown to depend on the fiber strength (related to processing) and work hardening behavior of the matrix. In Ti-6Al-4V (single step), most fractures occurred in the strain range 3–4%, where the work hardening rate is high. No fiber fractures occur after specimen necking. In Ti-14Al-21Nb/SCS-6, fiber fracture continued until the end since the WHR remained high until interruption by specimen fracture. In other words, the fragmentation did not saturate in that case. In fact, results in many other metal matrix composite systems are similar to this. The relationship between

fragment length and critical length in systems not showing saturation is not well understood. The WHR dependence will be most apparent when the fragments are getting shorter. Initially, residual and failure strain dominate.

Secondary fractures occur in all cases. These secondary fractures are due to shock-wave effect, as suggested previously.

Several improvements could be incorporated in future work, including specimen preparation to avoid damage to fiber, accurate measurement of residual stress–strain in the fiber, determination of *in-situ* strength of the fiber, AE signature and damage correlation by interrupted tests using AE source determination, wave form acquisition of AE signals, specimen nondestructive characterization by advanced ultrasonic techniques and correlation with metallography.

Acknowledgements

The contribution of Dr. S. Krishnamurthy in the fabrication and testing of the specimens is acknowledged. The results of AE work in this study are part of a collaborative effort between the author and Drs. I. Roman and M. C. Waterbury.

REFERENCES

1. A. Kelly and W. R. Tyson, Tensile properties of fiber-reinforced metals: copper/tungsten and copper/molybdenum, *J. Mech. Phys. Solids* **13**, 329–350 (1965).
2. J.-P. Favre and D. Jacques, Stress transfer in carbon fibre model composites, *J. Mater. Sci.* **25**, 1373–1380 (1990).
3. M. C. Waterbury and L. T. Drzal, On the determination of fiber strengths by *in-situ* fiber strength testing, *J. Comp. Tech. Res.* **13**, 22–28 (1991).
4. M. Narkis, E. J. H. Chen and R. B. Pipes, Review of methods for characterization of interfacial fiber–matrix interactions, *Polym. Compos.* **9**, 245–251 (1988).
5. R. B. Henstenburg and S. L. Phoenix, Interfacial shear strength studies using the single-filament-composite test. Part II: A probability model and Monte Carlo simulation, *Polym. Compos.* **10**, 389–408 (1989).
6. L. T. Drzal, M. Rich and P. Lloyd, Adhesion of graphite fibers to epoxy matrices. I. The role of fiber surface treatment, *J. Adhesion* **16**, 1–30 (1983).
7. W. A. Fraser, F. H. Ancker, A. T. DiBenedetto and B. Elbirli, Evaluation of surface treatments for fibers in composite materials, *Polym. Compos.* **4**, 238–248 (1983).
8. A. N. Netravali, R. B. Henstenburg, S. L. Phoenix and P. Schwartz, Interfacial shear strength studies using the single-filament-composite test. Part I: Experiments on graphite fibers in epoxy, *Polym. Compos.* **10**, 226–241 (1989).
9. R. P. Reed and J. C. Berg, Measuring effective interfacial shear strength in carbon fiber bundle polymeric composites, *J. Adhes. Sci. Technol.* **20**, 1929–1936 (2006).
10. F. G. Torres and M. L. Cubillas, Study of the interfacial properties of natural fibre reinforced polyethylene, *Polymer Testing* **24**, 694–698 (2005).
11. F. N. Nguyen and J. C. Berg, Use of an optical-mechanical test combined with acoustic-emission techniques to study adhesion in filled polymeric composites, *J. Adhesion* **81**, 823–841 (2005).
12. S. Ochiai and K. Osamura, Multiple fracture of a fibre in a single tungsten fibre–copper matrix composite, *Z. Metallkd.* **77**, 255–259 (1986).
13. L. Molliex, J.-P. Favre, A. Vassel and M. Rabinovitch, Interface contribution to the SiC-titanium and SiC-aluminium tensile strength prediction, *J. Mater. Sci.* **29**, 6033–6040 (1994).

14. R. B. Clough, F. S. Biancaniello, H. N. G. Wadley and U. R. Kattner, Fiber and interface fracture in single crystal aluminum/SiC fiber composites, *Metall. Trans.* **21A**, 2747–2757 (1990).
15. J.-L. Houpert, S. L. Phoenix and R. Raj, Analysis of the single-fiber-composite test to measure the mechanical properties of metal–ceramic interfaces, *Acta Metall. Mater.* **42**, 4177–4187 (1994).
16. A. Vassel, M. C. Merienne, F. Pautonnier, L. Molliex and J.-P. Favre, A method to evaluate the bonding between fibre and matrix in Ti-base composite, in: *Proc. of the 6th World Conference on Titanium*, P. Lacombe, R. Tricot and G. Beranger (Eds), pp. 919–923. Les Editions de Physique, Les Ulis Cedex, France (1988).
17. Y. Le Petitcorps, R. Pailler and R. Naslain, The fibre/matrix interfacial shear strength in titanium alloy matrix composites reinforced by silicon carbide or boron CVD filaments, *Compos. Sci. Technol.* **35**, 207–214 (1989).
18. I. Roman, S. Krishnamurthy and D. B. Miracle, Fiber–matrix interfacial behavior in SiC-titanium alloy composites, in: *Titanium '92 Science and Technology*, F. H. Froes and I. Caplan (Eds). The Minerals, Metals and Materials Society (1993).
19. X. J. Ning and P. Pirouz, Microstructure of SCS-6 SiC fiber, *J. Mater. Res.* **6**, 2234–2248 (1991).
20. C. G. Rhodes and R. A. Spurling, Fiber–matrix reaction zone growth kinetics in SiC-reinforced Ti-6Al-4V as studied by transmission electron microscopy, in: *Recent Advances in Composites in the United States and Japan*, J. R. Vinson and M. Taya (Eds), ASTM STP 864, pp. 585–599. ASTM, Philadelphia (1985).
21. L. W. Hall, J.-L. Lim, Y. Le Petitcorps and K. Bilba, Microstructural analysis of isothermally exposed Ti/SiC metal matrix composites, *J. Mater. Sci.* **27**, 3835–3842 (1992).
22. S. F. Baumann, P. K. Brindley and S. D. Smith, Reaction zone microstructure in a Ti_3Al + Nb/SiC composite, *Metall. Trans.* **21A**, 1559–1569 (1990).
23. W. P. Hon, S. K. Wu, and C. H. Koo, Tensile properties of a textured $Ti_{65}Al_{25}Nb_{10}$ alloy, *Mat. Sci. Engng.* **131A**, 85–91 (1991).